ELSEVIER

Catalysis Today 78 (2003) 281–290

CATALYSIS TODAY

www.elsevier.com/locate/cattod

Preparation of catalyst precursors for selective oxidation of *n*-butane by exfoliation–reduction of $VOPO_4{\cdot}2H_2O$ in primary alcohol

Yuichi Kamiya [a,*], Satoshi Ueki [a], Norihito Hiyoshi [b], Naoki Yamamoto [b], Toshio Okuhara [b,1]

[a] *Research and Development Center, Tonen Chemical Corporation, 3-1 Chidori-cho, Kawasaki-ku, Kawasaki 210-0865, Japan*

[b] *Graduate School of Environmental Earth Science, Hokkaido University, Sapporo 060-0810, Japan*

Abstract

A new method through intercalation and exfoliation of $VOPO_4{\cdot}2H_2O$ crystallites in primary alcohol (1-propanol or 1-butanol), followed by reduction with the alcohol, have been investigated for the preparation of catalyst precursor. Lamellar compounds, consisting of V^{4+}, P^{5+} and alkyl group with thin film-like morphology, were formed and was characterized by means of XRD, IR, TG/DTA, and elemental analysis. The chemical formula of the precursor obtained by exfoliation–reduction in 1-butanol was shown to be $VO\{(n\text{-}C_4H_9)_{0.16}H_{0.84}\}PO_4{\cdot}0.8H_2O$. On the other hand, a direct reduction of $VOPO_4{\cdot}2H_2O$ in the alcohol gave a mixed phase shown by $(VOHPO_4{\cdot}0.5H_2O)_{0.3}(VO\{(n\text{-}C_4H_9)_{0.3}H_{0.7}\}PO_4{\cdot}3H_2O)_{0.7}$ comprising plate-like microcrystallites. These precursors transformed to $(VO)_2P_2O_7$ phase during an activation process at 703 K in the presence of a mixture of *n*-butane 1.5% and O_2 17% in He balance. The obtained $(VO)_2P_2O_7$ through the exfoliation–reduction was well crystallized and consisted of thin flaky crystallites. It was found that $(VO)_2P_2O_7$ thus prepared through the exfoliation–reduction was highly active and selective for oxidation of *n*-butane.

Keywords: Vanadyl pyrophosphate; Vanadyl phosphate dihydrate; Exfoliation; Primary alcohol; *n*-Butane oxidation; Maleic anhydride

1. Introduction

Selective oxidation of *n*-butane to maleic anhydride (MA) is one of the commercialized applications in the gas-phase oxidation of lower alkanes with oxygen [1]. Vanadyl pyrophosphate, $(VO)_2P_2O_7$, is a main component of a commercial catalyst for this reaction [2–5]. One of the major problems in the commercial plant is the insufficient yield of MA. It is thus desirable to improve the yield by development of the catalytic performance.

Since the catalytic activity and selectivity of $(VO)_2P_2O_7$ are greatly dependent on the microstructure of the crystallites [6–8], control of the microstructure is critical for improvement of the catalytic performance. It is well known that vanadyl hydrogen phosphate hemihydrate, $(VOHPO_4{\cdot}0.5H_2O)$, a precursor for $(VO)_2P_2O_7$, can also be obtained by

* Corresponding author. Tel.: +81-44-266-1041; fax: +81-44-266-4562.
E-mail addresses: kamiya@exxonmobil.com (Y. Kamiya), oku@ees.hokudai.ac.jp (T. Okuhara).
[1] Tel./fax: +81-11-706-4513.

0920-5861/02/$ – see front matter © 2002 Elsevier Science B.V. All rights reserved.
PII: S0920-5861(02)00319-X

reduction of $VOPO_4{\cdot}2H_2O$ with alcohol [9]. Hutchings and coworkers [10,11] reported that the morphology of the precursor could be controlled by a choice of alcohol used as reducing agent.

Exfoliation technique has been developed from intercalation of various layered materials like clay [12], zirconium phosphate [13], niobates [14], and titanates [15], in which exfoliation is a method delaminating stacked inorganic sheets in solvent by infinite swelling of their interlayer space. $VOPO_4{\cdot}2H_2O$ is one of the layered compounds and possesses a high intercalating capability [16]. Recently, we found that intercalation and exfoliation of $VOPO_4{\cdot}2H_2O$ crystallites proceeded with a stepwise heating below refluxing temperature in 2-butanol and the subsequent reduction of the exfoliated $VOPO_4{\cdot}2H_2O$ brought about $VOHPO_4{\cdot}0.5H_2O$ crystallites of thin sheet [17]. Furthermore, $(VO)_2P_2O_7$ obtained from the precursor was highly active and selective for the selective oxidation of *n*-butane [17].

In the present study, we aimed at preparing the precursor and catalyst through intercalation, exfoliation and reduction of $VOPO_4{\cdot}2H_2O$ in primary alcohol. The obtained crystallites have been systematically characterized in order to elucidate the features of this preparation method. Furthermore, the catalytic property for the selective oxidation of *n*-butane has been examined, comparing with that of conventional catalyst.

2. Experimental

2.1. Preparation of precursors

$VOPO_4{\cdot}2H_2O$ was prepared according to the literature [16]. A mixture of V_2O_5 (24 g, Wako Pure Chemical Ind.) and 85% H_3PO_4 (133 cm^3, Wako Pure Chemical Ind.) and H_2O (577 cm^3) was refluxed at 388 K for 16 h to form precipitates. The obtained solid was filtered, washed with acetone, and dried at room temperature for 16 h. The solid was confirmed to be $VOPO_4{\cdot}2H_2O$ by XRD and IR. $VOPO_4{\cdot}2H_2O$ (0.5 g) was added to 1-propanol or 1-butanol (50 cm^3, Wako Pure Chemical Ind.) at room temperature. The suspension was stepwise heated at room temperature, 303, 323, or 343 K for 1 h at each temperature. Then the solution was further refluxed at 363 K (1-propanol) or 383 K (1-butanol) for 24 h to obtain light-blue precipitates. The obtained solids from 1-propanol and 1-butanol are denoted EP(1-Pr) and EP(1-Bu), respectively.

As a reference, the precursors were separately prepared by the conventional methods, e.g. the direct reduction of $VOPO_4{\cdot}2H_2O$ with alcohol [11] and the organic solvent method [8]. For the direct reduction, $VOPO_4{\cdot}2H_2O$ (5.0 g) was added to 1-propanol, 1-butanol or 2-butanol (50 cm^3, Wako Pure Chemical Ind.) at room temperature, followed by refluxed at 363 K (1-propanol) or 383 K (1-butanol and 2-butanol) for 18 h. The solids obtained from 1-propanol, 1-butanol and 2-butanol are denoted P(1-Pr), P(1-Bu) and P(2-Bu), respectively. For the organic solvent method, the precursor $VOHPO_4{\cdot}0.5H_2O$ (denoted as P-3) was prepared using isobutyl alcohol and benzyl alcohol [8], and the corresponding $(VO)_2P_2O_7$ (denoted as C-3) was obtained by the calcination at 773 K in 9.1% O_2 (He balance).

2.2. Characterization

Powder XRD patterns were obtained on an X-ray diffractometer (Rigaku Miniflex) with Cu Kα radiation ($\lambda = 0.154$ nm). Infrared spectra were recorded with an IR spectrometer (Bio-rad FTS-7) by a KBr method. SEM images were taken by using a Hitachi S-2100A scanning electron microscope. Thermogravimetric analysis (TG/DTA) was performed in a flow of dry air (100 $cm^3\,min^{-1}$) by using a Seiko Instruments TG/DTA-6300. The sample was heated from 303 to 853 K at a rate of 10 $K\,min^{-1}$.

Elemental analysis of the samples for C and H were carried out at the Center for Instrumental Analysis, Hokkaido University. The contents of V and P were determined by an inductively coupled plasma-atomic emission spectrometer (ICP-AES, Shimadzu ICPS-8000), in which the sample powder was dissolved into hot H_2SO_4, and the solution was diluted with water to about 30 ppm of V and P. The content of oxygen in the sample was calculated by subtracting the sum of weights of V, P, C, and H.

The average oxidation number of V was determined by a redox titration method according to the literature [18]. The surface area was measured by a BET method with automatic adsorption system (BELSORP 28SA, BEL Japan).

2.3. Catalytic oxidation of n-butane

Catalytic oxidation of *n*-butane was performed in a flow reactor (Pyrex tube, inside diameter of 10 mm) under an atmospheric pressure at 703 K using a mixture consisting of *n*-butane 1.5 vol.%, O_2 17 vol.%, and He (balance). The precursor was activated in the reactant mixture by heating from room temperature to 703 K at a rate of 10 K min^{-1}. The products were analyzed with gas chromatographs, an FID-GC (Shimadzu 8A) equipped with Porapak QS column for *n*-butane and MA, and a high speed GC (TCD, Area Japan M-200) with Porapak Q and Molecular Sieves 5A columns for O_2, CO, and CO_2. The catalysts derived from EP(1-Bu) and P(1-Bu) are denoted EC(1-Bu) and C(1-Bu), respectively.

3. Results and discussion

3.1. Catalyst precursors obtained through exfoliation of $VOPO_4{\cdot}2H_2O$

When the powder of $VOPO_4{\cdot}2H_2O$ (lemon yellow) was stepwise heated in 1-butanol at room temperature, 303, 323, and 343 K for 1 h at each temperature, the alcohol suspension became homogeneous yellow solution. By evaporating the resulting homogeneous solution at 333 K, a yellow-green powder was formed. XRD pattern and IR spectrum of the solid were the same as those of the starting $VOPO_4{\cdot}2H_2O$ (the data were not shown). As will be discussed elsewhere [17,19,20], $VOPO_4$ sheets were delaminated in 1-butanol solution (exfoliation). Subsequent refluxing

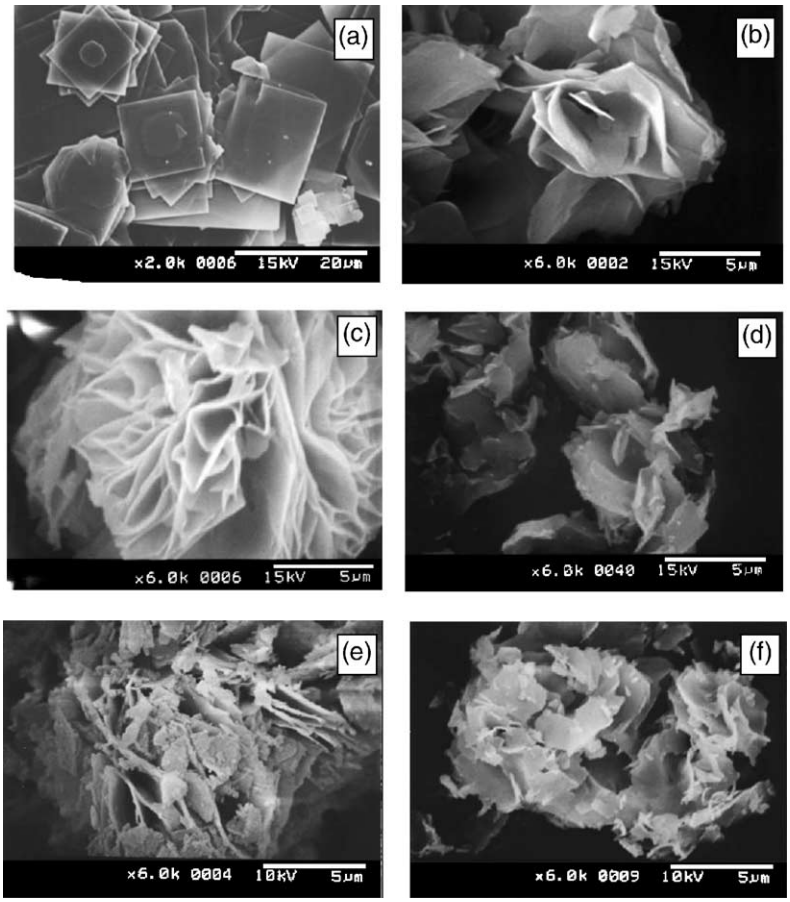

Fig. 1. SEM micrographs of vanadium phosphorus oxides: (a) $VOPO_4{\cdot}2H_2O$; (b) EP(1-Pr); (c) EP(1-Bu); (d) P(1-Bu); (e) EC(1-Bu); (f) C(1-Bu).

Table 1
Elemental analysis and average oxidation number of vanadium for the precursors obtained from $VOPO_4{\cdot}2H_2O$ in 1-butanol

Precursor[a]	V (wt.%)[b]	P (wt.%)[b]	C (wt.%)[b]	H (wt.%)[b]	O (wt.%)[b,c]	Average oxidation number of V	Formula
EP(1-Bu)	24.79 (1.00)	15.83 (1.05)	3.76 (0.64)	2.95 (6.01)	52.67 (6.76)	3.95	$VO\{(C_4H_9)_{0.2}H_{0.8}\}PO_4{\cdot}0.8H_2O$
P(1-Bu)	25.12 (1.00)	15.95 (1.04)	1.93 (0.33)	2.23 (4.49)	54.77 (6.94)	4.05	$(VOHPO_4{\cdot}0.5H_2O)_{0.3}$ $(VO\{(C_4H_9)_{0.3}H_{0.7}\}$ $PO_4{\cdot}2H_2O)_{0.7}$

[a] EP(1-Bu) and P(1-Bu) were obtained by exfoliation–reduction and direct reduction of $VOPO_4{\cdot}2H_2O$ in 1-butanol, respectively.
[b] The figures in parentheses are relative atomic ratios.
[c] Oxygen content was estimated by subtracting the sum of weights of V, P, C, and H.

the exfoliation solution for 24 h produced light-blue precipitates. Also in the case of 1-propanol, a homogeneous alcoholic solution was obtained and light-blue precipitate was formed by further refluxing.

SEM micrographs are shown in Fig. 1. The starting $VOPO_4{\cdot}2H_2O$ consisted of square platelets with the lateral dimensions of about 10 μm and thickness of about 1 μm (Fig. 1a). As Fig. 1b and c shows, the precursor obtained by intercalation, exfoliation, and reduction (EP(1-Pr) and EP(1-Bu)) consists of thin films (thickness; less than 0.1 μm) randomly gathered. On the other hand, P(1-Bu) was aggregates of plate-like microcrystallites (Fig. 1d).

Table 1 summarizes the results of the elemental chemical analysis of EP(1-Bu) and P(1-Bu), together with average oxidation numbers of V. The P/V ratios of both precursors were nearly unity and the average oxidation numbers were about +4.0. The R/P ratio of EP(1-Bu) estimated from the C/P ratio was 0.16 (R = *n*-C_4H_9), indicating *n*-butyl group is incorporated in EP(1-Bu). The R/P ratio of P(1-Bu) was 0.08, which was less than that of EP(1-Bu).

Fig. 2 shows the XRD patterns of starting $VOPO_4{\cdot}2H_2O$ and the obtained precursors. The XRD pattern of P(2-Bu) corresponds to that of $VOHPO_4{\cdot}0.5H_2O$ with characteristic XRD lines (Fig. 1f) [21]. As shown in Fig. 2b and c, the XRD patterns of the precursors obtained by the exfoliation–reduction process differ from that of P(2-Bu). EP(1-Pr) and EP(1-Bu) gave intense peaks at less than 10° of 2θ, suggesting a lamellar compound with intercalated alcohol molecules. Assuming that these intense peaks correspond to a diffraction from the (0 0 1) plane, the basal spacings (d_{001}) are estimated to be 0.98 and 1.07 nm for EP(1-Pr) and EP(1-Bu), respectively, and these values are larger than that of $VOPO_4{\cdot}2H_2O$ (0.74 nm) (Fig. 2a). The XRD patterns show peaks assignable to the (0 0 2) lines at 18.2° (0.49 nm) for EP(1-Pr) and 16.6° (0.53 nm) for EP(1-Bu), respectively. Molecular lengths of 1-propanol and 1-butanol are 0.464 and 0.596 nm, respectively, where the molecular length as the distance between O and H of $-CH_3$ is estimated on the basis of the covalent bond length with MOPAC (FUJITSU, WinMOPAC Ver. 3.0). Since the d_{001} value of EP(1-Bu) is larger than that of EP(1-Pr), it is considered that the alkyl groups play an essential role in constructing the lamellar structure.

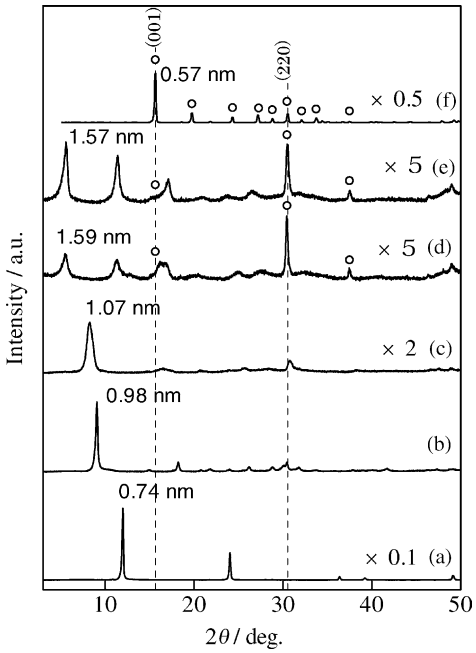

Fig. 2. XRD patterns of vanadium phosphorus oxides: (a) $VOPO_4{\cdot}2H_2O$; (b) EP(1-Pr); (c) EP(1-Bu); (d) P(1-Pr); (e) P(1-Bu); (f) P(2-Bu). (○) $VOHPO_4{\cdot}0.5H_2O$.

The precursors obtained by direct reduction in 1-propanol and 1-butanol also gave typical patterns due to lamellar compound (Fig. 2d and e). The $d_{0\,0\,1}$ values for P(1-Pr) and P(1-Bu) were 1.59 and 1.57 nm, respectively, which were larger than those of EP(1-Pr) and EP(1-Bu). Since $d_{0\,0\,1}$ value changed scarcely when 1-butanol was used instead of 1-propanol, the size of alkyl group dose not influence the basal spacing. For P(1-Pr) and P(1-Bu), a strong sharp line at 30.52° of 2θ was observed, which agrees with a diffraction of the (2 2 0) plane for $VOHPO_4{\cdot}0.5H_2O$. Furthermore, an XRD line at 15.64° assigned to the (0 0 1) line for $VOHPO_4{\cdot}0.5H_2O$ was observed. Hutchings and coworkers [11] reported that similar process produced $VOHPO_4{\cdot}0.5H_2O$ with a specific VPD ($VOPO_4{\cdot}2H_2O$ route) morphology which favor thin platelets in the [0 0 1] direction. Therefore, it is deduced that P(1-Pr) and P(1-Bu) is a mixture of $VOHPO_4{\cdot}0.5H_2O$ and the lamellar compound.

Infrared spectra of $VOPO_4{\cdot}2H_2O$ and the precursors are given in Fig. 3. The spectrum of P(2-Bu) are consistent with that of $VOHPO_4{\cdot}0.5H_2O$ (Fig. 3d) [7]. The bands for P(2-Bu) were assigned to $\nu(PO_3)$ for 1197, 1103, and 1055 cm^{-1}, δ(P–OH) for 1131 cm^{-1}, ν(V=O) for 977 cm^{-1}, and ν(P–OH) for 932 cm^{-1} [7]. All precursors gave similar spectra to that of $VOHPO_4{\cdot}0.5H_2O$ in lattice vibration region (less that 1500 cm^{-1}), indicating that a structure of V–P–O layer for the precursors is analogous to that of $VOHPO_4{\cdot}0.5H_2O$. For EP(1-Bu), the bands at 1183, 1087, and 1062 cm^{-1} are assigned to $\nu(PO_3)$ and 982 cm^{-1} to ν(V=O) (Fig. 3b). In addition, the band at 933 cm^{-1} (shoulder) is assignable to ν(P–OH). The P(1-Bu) displayed similar bands to P(2-Bu) in lattice vibration region, although the bands were broadened. EP(1-Bu) and P(1-Bu) gave a broad band over 3000 cm^{-1}, which is similar to $VOPO_4{\cdot}2H_2O$ (Fig. 3a), due to water weakly held in interlayer space.

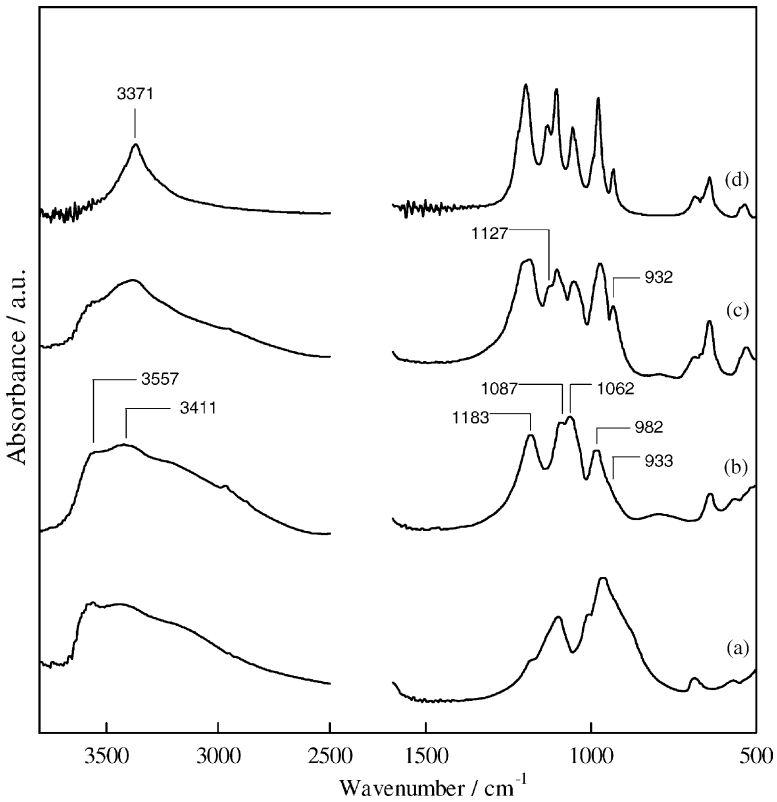

Fig. 3. Infrared spectra of vanadium phosphorus oxides: (a) $VOPO_4{\cdot}2H_2O$; (b) EP(1-Bu); (c) P(1-Bu); (d) P(2-Bu).

TG/DTA profiles of EP(1-Bu), P(1-Bu) and P(2-Bu) are illustrated in Fig. 4. As shown in Fig. 4a, the sharp weight loss with endothermic below 450 K and loose weight loss with exothermic above 500 K were observed for EP(1-Bu). The initial weight loss may be attributed to loss of intercalated water molecules. Considering the exothermic and relatively high temperatures, the weight loss above 500 K is probably due to combustion of *n*-butyl group connected by a covalent bond. From these results, the chemical formula of EP(1-Bu) was estimated to be $VO\{(n\text{-}C_4H_9)_{0.16}H_{0.84}\}PO_4\cdot 0.8H_2O$. For P(1-Bu), the weight decreased in three steps at temperature range of (1) below 400 K, (2) 400–570 K, and (3) above 570 K (Fig. 4b). Endothermic valley observed at 650 K is attributed to transformation from $VOHPO_4\cdot 0.5H_2O$ to $(VO)_2P_2O_7$ as shown for P(2-Bu) (Fig. 4c). Since P(1-Bu) is a mixture of $VOHPO_4\cdot 0.5H_2O$ and the lamellar compound, the chemical formula of P(1-Bu) is described as $(VOHPO_4\cdot 0.5H_2O)_x\cdot(VO((C_4H_9)_y/H_{1-y})PO_4\cdot nH_2O)_{1-x}$. We estimated $x = 0.3$, $y = 0.3$, and $n = 3$ to satisfy the elemental analysis and TG result as listed in Table 1.

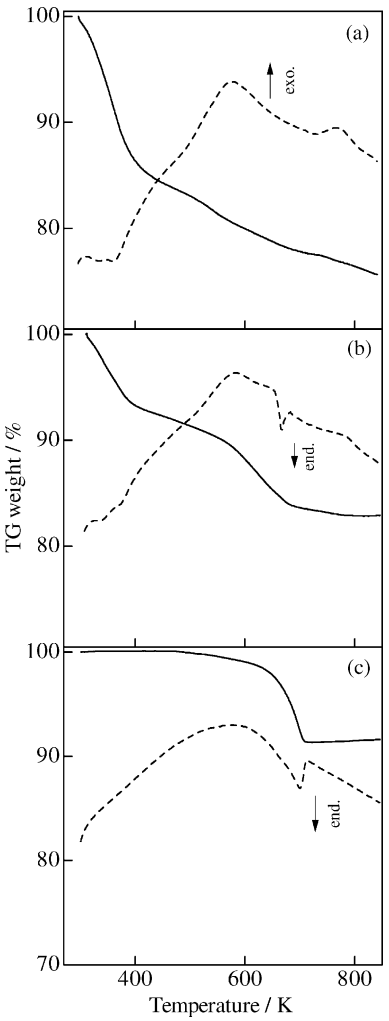

Fig. 4. TG/DTA profile of vanadium phosphorus oxides in air: (a) EP(1-Bu); (b) P(1-Bu); (c) P(2-Bu).

Based on these results, the schematic structures of EP(1-Bu) and P(1-Bu) are depicted in Fig. 5. The structure of V–P–O layer for both precursors is similar to $VOHPO_4\cdot 0.5H_2O$. For EP(1-Bu), the alkyl group plays an essential role in constructing the lamellar structure. P(1-Bu) is a mixture of $VOHPO_4\cdot 0.5H_2O$ and lamellar compound. The interlayer space of the lamellar compound is fulfilled with intercalated water molecules to form the lamellar structure. That may be a reason that the basal spacing of these compounds is not affected by the size of the alkyl groups.

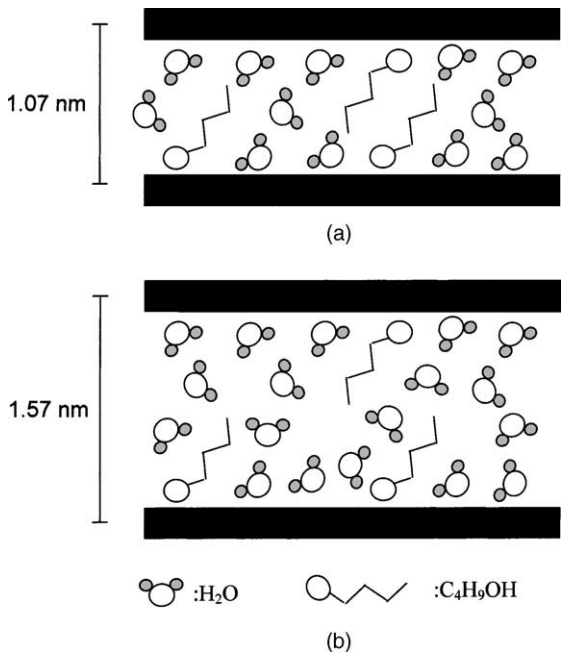

Fig. 5. Schematic structure of (a) EP(1-Bu) and (b) P(1-Bu).

3.2. Catalytic oxidation of n-butane

Fig. 6 shows the time course of the oxidation of *n*-butane over EC(1-Bu) and C(1-Bu). In order to adjust the conversion, the reactions were performed in the different reaction conditions, i.e. W/F = 120 g h mol^{-1} for EC(1-Bu), and 163 g h mol^{-1} for C(1-Bu), respectively (W = catalyst weight (g), and F = flow rate of *n*-butane (mol h^{-1})). As shown in Fig. 6, the conversion and selectivity to MA increased at the initial stage of the reaction over both C(1-Bu) and EC(1-Bu). The stationary values were obtained after about 80 h of the reaction, indicating that these catalysts were equilibrated. Thus the reaction rate and selectivity were determined from the data collected around 100 h.

Fig. 7 presents *W*/*F* dependence of the conversion of *n*-butane. The activity of EC(1-Bu) is high compared with that of C(1-Bu).

Fig. 8 gives the change in the selectivity to MA as a function of the conversion of *n*-butane. Fig. 8 demonstrates that EC(1-Bu) is more selective than C(1-Bu). In addition, it is noted that the selectivity to MA was higher than 70% at low conversions over EC(1-Bu).

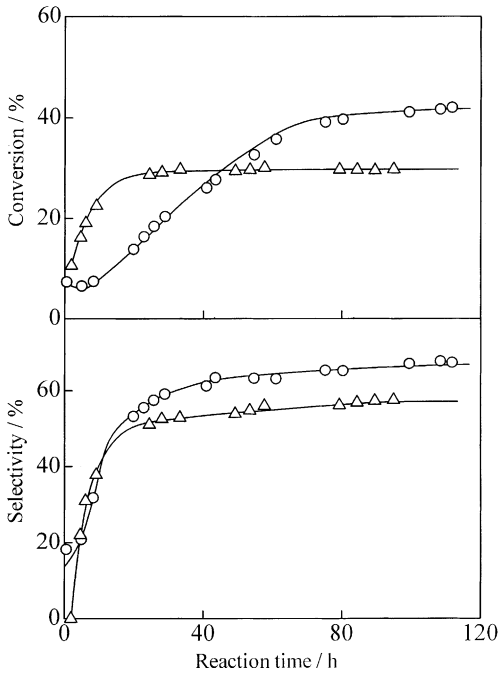

Fig. 6. Changes of the conversion and selectivity to MA in the oxidation of *n*-butane over various V–P oxide catalysts: (○) EC(1-Bu); (△) C(1-Bu). The reaction was performed at 703 K with *n*-butane (1.5%), O_2 (17%), and He (balance). W/F = 120 and 163 g h mol^{-1} for EC(1-Bu), and C(1-Bu), respectively.

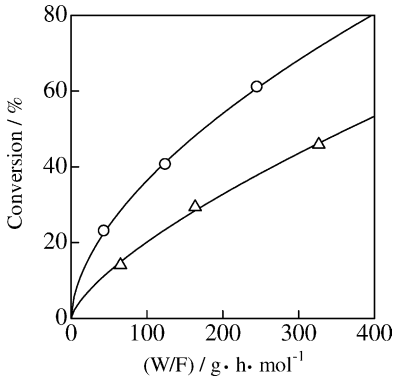

Fig. 7. Dependence of the conversion of *n*-butane on the contact time: (○) EC(1-Bu); (△) C(1-Bu). The reaction was performed at 703 K with *n*-butane (1.5%), O_2 (17%), and He (balance).

In Table 2, the catalytic data are summarized. From the slope of the curve at low *W*/*F* region (less than 80 g h mol^{-1}) in Fig. 7, the reaction rate was determined. The great difference in the catalytic activity for EC(1-Bu) and C(1-Bu) is attributed to the difference in the surface area, since the specific activity defined as the rate per surface area was comparable with each other. It should be noted that EC(1-Bu) was more active than C-3, which is known to be effective for the *n*-butane oxidation [1,4,8]. The selectivity of EC(1-Bu) was comparable to that of C-3.

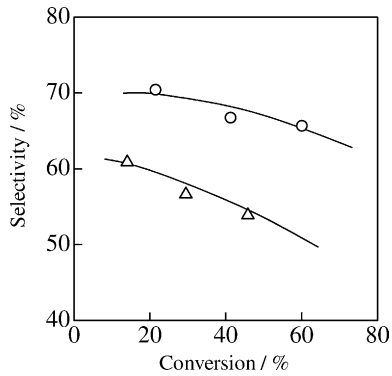

Fig. 8. Selectivity to MA as a function of the conversion of *n*-butane: (○) EC(1-Bu); (△) C(1-Bu). The reaction was performed at 703 K with *n*-butane (1.5%), O_2 (17%), and He (balance).

Table 2
Surface area, size of crystallites and catalytic performance of V–P oxides for oxidation of *n*-butane[a]

Catalyst[b]	Surface area[c] ($m^2\ g^{-1}$)	Size of crystallites (nm)			Rate ($\times 10^{-4}$ mol $g^{-1}\ h^{-1}$)	Selectivity to MA[d] (%)	
		Length	D_{SA}[e]	D_{XRD}[f]		20%[g]	50%[g]
EC(1-Bu)	41	1000	15	20	60 (1.5)[h]	71	67
C(1-Bu)	22	3000	29	7	26 (1.2)[h]	59	53
C-3	36	–	–	–	24 (0.7)[h]	–	72[i]

[a] The reaction was performed with a mixture of *n*-butane (1.5%), O_2 (17%), and He (balance) at 703 K.
[b] EC(1-Bu) and C(1-Bu) were obtained from EP(1-Bu) and P(1-Bu), respectively, and C-3 is $(VO)_2P_2O_7$ prepared by organic solvent method.
[c] Surface area after the reaction.
[d] Selectivity based on *n*-butane.
[e] Thickness estimated from surface area and density of $(VO)_2P_2O_7$.
[f] Thickness estimated with Scherrer's equation [22].
[g] Conversion of *n*-butane.
[h] Rate per surface area ($\times 10^{-4}$ mol $m^{-2}\ h^{-1}$).
[i] Selectivity at 56% of the conversion.

As shown in Fig. 1, the crystallites of EP(1-Bu) were fractured to small flaky crystallites by the calcination under the reaction condition (Fig. 1e). On the other hand, the plate-like morphology of C(1-Bu) (Fig. 1f) was basically kept to that of the precursor (Fig. 1d).

Powder XRD patterns and IR spectra of the catalysts after the reaction are shown in Fig. 9. Both EC(1-Bu) and C(1-Bu) gave XRD diffraction lines only due to $(VO)_2P_2O_7$ (Fig. 9A). However, the difference in the line-width was detected between these catalysts; EC(1-Bu) gave more sharp lines. As shown in Fig. 9B, EC(1-Bu) gave IR bands at 632 cm^{-1} ($\delta(PO_3)$), 744 cm^{-1} (ν(P–O–P)), 796 cm^{-1} (ν(V–O=V)), 970 cm^{-1} (ν(V=O)), and 1092, 1143, 1220, and 1239 cm^{-1} ($\nu(PO_3)$) [7]. Contrary to EC(1-Bu), the bands at 1099 and 1220 cm^{-1} ($\nu(PO_3)$)were weak for C(1-Bu). XRD and IR data suggest that the crystallinity of EC(1-Bu) is higher than that for C(1-Bu).

The size of crystallites and surface area are summarized in Table 2. The surface area of EC(1-Bu) was about two times higher than that of C(1-Bu). As

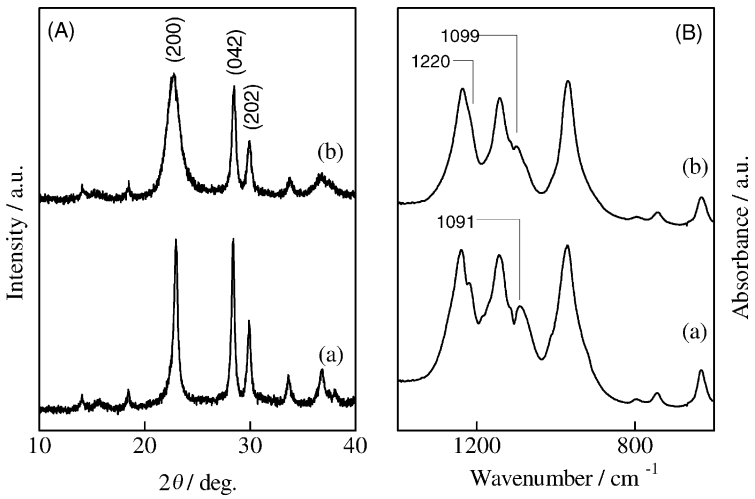

Fig. 9. XRD patterns (A, left) and IR spectra (B, right) of V–P oxide catalysts after the reaction: (a) EC(1-Bu); (b) C(1-Bu).

will be discussed below, the thinner microcrystallites are formed by the exfoliation–reduction method. Thus the resulting crystallites have high surface area. The thickness of the crystallites was estimated from surface area using Eq. (1) or from the XRD line-width of the (2 0 0) line using Scherrer's Eq. (2) [22]:

$$\frac{2}{D_{SA}} + \frac{4}{L} = S\rho \quad (1)$$

$$D_{XRD} = \frac{\alpha\lambda}{\Delta 2\theta \cos\theta_0} \quad (2)$$

In Eq. (1), D_{SA} is the thickness of the crystallite, L the length of the crystallite, S the surface area, and ρ the density (3.34×10^{-12} g μm^{-3}) of $(VO)_2P_2O_7$ [23]. In Eq. (2), D_{XRD} is the thickness of the crystallite, α a constant (1.0), $\Delta 2\theta$ the line-width of the (2 0 0) line, and θ_0 the angle of the (2 0 0) line.

D_{SA} of EC(1-Bu) was estimated to be 15 nm which is approximately the same as D_{XRD} (20 nm). On the other hand, D_{SA} (29 nm) of C(1-Bu) was greatly different from D_{XRD} (7 nm). When XRD lines are broadened by a structural disorder in the sample solid, the Scherrer's equation is considered to underestimate a size of crystallites. C(1-Bu) gave broad lines in XRD, although D_{SA} of C(1-Bu) is larger than that of EC(1-Bu). P(1-Bu) contains larger quantities of alkyl groups and water molecules and larger $d_{0\,0\,1}$ value compared with EP(1-Bu), which may induce the structural disorder in C(1-Bu) in the transformation of P(1-Bu) to C(1-Bu). This is the reason for the broader XRD lines for C(1-Bu). Therefore, we chose D_{SA} to estimate the thickness. The thickness of EC(1-Bu) was about half of that of C(1-Bu), resulting in the higher surface area of EC(1-Bu).

Okuhara and coworkers [6] reported that the basal plane of $(VO)_2P_2O_7$, on which characteristic pair sites (V^{4+}–O–V^{4+}) are located, is selective for MA formation, but the side planes are non-selective for the selective oxidation of *n*-butane. Since EC(1-Bu) consisted of thin flaky crystallites, the basal plane was more exposed on EC(1-Bu) as compared with C(1-Bu). Therefore, one of the reason for the high selectivity of EC(1-Bu) is the influence of the greater extent of the fraction of the basal plane. In addition, the nature of the basal plane of EC(1-Bu) would be preferable for the selective formation of MA. These results demonstrate that the present method utilizing intercalation, exfoliation and reduction of $VOPO_4{\cdot}2H_2O$ in primary alcohol is useful for the development of efficient catalyst.

4. Conclusion

Powder of $VOPO_4{\cdot}2H_2O$ was exfoliated by stepwise heating in 1-butanol. The obtained precursor was a lamellar compound and the chemical formula was $VO\{(n\text{-}C_4H_9)_{0.16}H_{0.84}\}PO_4{\cdot}0.8H_2O$ with randomly gathered thin film. The precursor was transformed to $(VO)_2P_2O_7$ consisting of thin flaky crystallites during an activation process at 703 K in the presence of a reaction mixture. The catalyst showed high activity and selectivity for the selective oxidation of *n*-butane in comparison with the catalyst obtained by the direct reduction of $VOPO_4{\cdot}2H_2O$.

Acknowledgements

This work was supported by the New Energy and Industrial Technology Development Organization (NEDO) and Japan Chemical Industry Association (JCIA).

References

[1] S. Albonetti, F. Cavani, F. Trifirò, Catal. Rev.-Sci. Eng. 38 (1996) 413.
[2] E. Bordes, Catal. Today 1 (1987) 499.
[3] G.J. Hutchings, Appl. Catal. 72 (1991) 1.
[4] G. Centi, F. Trifirò, J.R. Ebner, V.M. Franchetti, Chem. Rev. 88 (1988) 55.
[5] B.K. Hodnett, Catal. Rev.-Sci. Eng. 27 (1985) 373.
[6] K. Inumaru, T. Okuhara, M. Misono, Chem. Lett. (1992) 947.
[7] G. Busca, F. Cavani, G. Centi, F. Trifirò, J. Catal. 99 (1986) 400.
[8] Y. Kamiya, E. Nishikawa, T. Okuhara, T. Hattori, Appl. Catal. A 206 (2001) 103.
[9] J.W. Johnson, D.C. Johnston, A.J. Jacobson, J.F. Brody, J. Am. Chem. Soc. 106 (1984) 8123.
[10] I.J. Ellison, G.J. Hutchings, M.T. Sananes, J.C. Volta, J. Chem. Soc., Chem. Commun. (1994) 1093.
[11] M.T. Sananes, I.J. Ellison, S. Sajip, A. Burrows, C.J. Kiely, J.C. Volta, G.J. Hutchings, J. Chem. Soc., Faraday Trans. 92 (1996) 137.
[12] E.R. Kleinfeld, G.S. Furgson, Science 265 (1994) 370.
[13] S.W. Kelle, H.-N. Kim, T.E. Mallouk, J. Am. Chem. Soc. 116 (1994) 8817.

[14] R. Abe, K. Shinohara, A. Tanaka, M. Hara, J.N. Kondo, K. Domen, Chem. Mater. 9 (1997) 2179.
[15] T. Sakaki, S. Nakano, S. Yamauchi, M. Watanabe, Chem. Mater. 9 (1997) 602.
[16] G. Ladwig, Z. Anorg. Allg. Chem. 338 (1965) 266.
[17] N. Hiyoshi, N. Yamamoto, T. Okuhara, Chem. Lett. (2001) 484.
[18] B.K. Hodnett, P. Permanne, B. Delmon, Appl. Catal. 6 (1983) 231.
[19] T. Nakato, Y. Furumi, T. Okuhara, Chem. Lett. (1998) 611.
[20] N. Yamamoto, N. Hiyoshi, T. Okuhara, Chem. Mater. 14 (2002) 3882.
[21] H. Igarashi, K. Tsuji, T. Okuhara, M. Misono, J. Phys. Chem. 97 (1993) 7065.
[22] P. Scherrer, Göttinger Nachrichem 2 (1918) 98.
[23] P.T. Nguyen, R.D. Hoffman, A.W. Sleight, Mater. Res. Bull. 30 (1995) 1055.